



HAL
open science

Acoustic liner demonstrator for a turning vane of S1MA wind tunnel

Fabien Méry, Rémi Roncen, Frank Simon, Marlon Botte, Loïc Ostorero

► **To cite this version:**

Fabien Méry, Rémi Roncen, Frank Simon, Marlon Botte, Loïc Ostorero. Acoustic liner demonstrator for a turning vane of S1MA wind tunnel. *Journal of Aircraft*, 2023, 60 (4), pp.1314-1322. 10.2514/1.C037048 . hal-04021941

HAL Id: hal-04021941

<https://hal.science/hal-04021941>

Submitted on 9 Mar 2023

HAL is a multi-disciplinary open access archive for the deposit and dissemination of scientific research documents, whether they are published or not. The documents may come from teaching and research institutions in France or abroad, or from public or private research centers.

L'archive ouverte pluridisciplinaire **HAL**, est destinée au dépôt et à la diffusion de documents scientifiques de niveau recherche, publiés ou non, émanant des établissements d'enseignement et de recherche français ou étrangers, des laboratoires publics ou privés.

Acoustic liner demonstrator for a turning vane of S1MA windtunnel

Fabien Méry^{*†} and Rémi Roncen[‡] and Frank Simon[§]
ONERA/DMPE–Toulouse University, F-31055 Toulouse, France

Marlon Botte[¶] and Loïc Ostorero^{||}
ONERA/DSMA, F-73500 Modane, France

I. Introduction

Aerodynamic measurements are usually performed in closed-section wind tunnels while acoustic tests are preferably conducted in anechoic open-section wind tunnels. Indeed, open-section wind tunnels enable out-of-flow acoustic measurements and due to the large dimensions of such facilities, these measurements are usually free from any reverberation effects. However, the aerodynamic capabilities are limited in an open-section wind tunnel, and the Mach number range is more limited than in a closed-section configuration. Furthermore, out-of-flow measurements are limited in frequency due to the haystacking phenomena that occurs when waves travel through the shear layer separating the uniform flow region from the fluid at rest. From a different point of view, using the same facility for both acoustics and aerodynamics is financially attractive but challenging since only in-flow measurements can be performed in this case. Current constraints on the design, in terms of aircraft noise, evolve and become paramount issues. So far, only takeoff and landing conditions are studied using open-jet anechoic facilities. Now, cabin noise and, by extension, acoustic cruising conditions are becoming increasingly important. The complexity of the phenomena requires an investigation in experimentation techniques to develop future aircrafts. The development of innovative engines such as the Open Rotor concept or UHBR (Ultra High Bypass Ratio) turbofans provides new opportunities for research and development in the field of aeroacoustics.

While the noise reduction devices or design in an aeronautical context are more and more efficient i.e. making less noise, it is important to adapt the metrology in order to address these challenges. Three major directions are generally used in order to improve the signal-to-noise ratio in a given facility : signal processing enhancement, instrumentation development and facility improvement. These three directions are sorted by increasing investment. De-noising techniques (thanks to signal processing) have been featured by Chung [1], who proposed an approach based on three sensors, with one sensor near the acoustic sources, enabling noise rejection due to the facility and thus de-noise the far

*Presented as Paper 2022-2855 at the 2022 AIAA/CEAS Aeroacoustics Conference, Southampton, UK, 14–17 June 2022

†PhD, DMPE, fabien.mery@onera.fr

‡PhD, DMPE, remi.roncen@onera.fr

§PhD, DMPE, frank.simon@onera.fr

¶Ing, DSMA, marlon.botte@onera.fr

|| Ing, DSMA, loic.ostorero@onera.fr

field sound field. Several other recent and more complex signal processing approaches can be also highlighted [2, 3]. The instrumentation hardware design is also an important element in order to avoid the effect of spurious noise due to the instrumentation installation. Screened-recessed microphones [4, 5] remain a good strategy when combined with a robust signal processing : the spurious noise due to pseudo-sound is filtered by this screening that involves the usage of wiremesh or kevlar. Finally, the improvement of the facility itself is mandatory to accurately measure low-noise aerodynamic devices. Several worldwide facilities have incorporated modifications in order to reduce test section background noise [6, 7]. These modifications include optimisation of the fan, the redesign and lining of the corner turning vane and the redesign of the turbulence filter.

ONERA offers the world largest transonic wind tunnel facility, S1MA, where experiments using large scale models can be performed. This facility gives the opportunity to carry out both aerodynamic tests and acoustic tests since it has an anechoic test section and can reach a Mach number of 0.3 [8]*. This facility is ideal for far-field aeroacoustic studies of large and complex models. It gives a complete tool for aerodynamic and aeroacoustic development of future engines. Several aeroacoustic instrumentation developments [9] were performed, not only to consider the reverberation effect due to measurement in a closed test section, but also to improve signal-to-noise ratio [10], which is a paramount topic in aeroacoustic measurement. Several post-processing strategies dedicated to the Open Rotor issue have been applied [11] in order to de-noise the measurements. These approaches make sense when the studied specimen has an harmonic reference that enables extraction through resynchronization and removes noise from the signal (the blade passing fan frequency is directly linked to the RPM of the model). In order to study the effects of a broadband noise source, the general background noise of the installation should be reduced (which has significant broadband content). The methodology should rely on several numerical design tools and experimental assessment of the solution in order to guide the decision-maker. The first part of this article will present the facility and the selected strategy to reduce background noise by modifying the turning vane. The second part is dedicated to liner design and optimisation and several simulations that will be a key driver in the selection of the configurations to be tested. Finally, a demonstrator will be manufactured and assessed. The experimental set up and the signal processing are described and the results of the different solutions are finally analyzed.

II. Background noise reduction challenge in S1MA Large wind tunnel facility

The ONERA S1MA wind tunnel (Fig. 1) is the world largest sonic tunnel with a test section 8 m in diameter and 14 m long. It is operated at ONERA's Modane test centre in the French Alps. The tunnel consists of a settling chamber with a contraction leading to the tunnel test section followed by a diffuser, two hydraulic contra-rotating fans and a return leg leading to the settling chamber. Each contra-rotating fan (15 m in diameter) is directly driven by one Pelton turbine and total hydraulic power is equal to 88 MW. This direct hydraulic drive is a great advantage from the viewpoint

*when performing acoustic testing in the anechoic test section, this limiting Mach number has to be considered

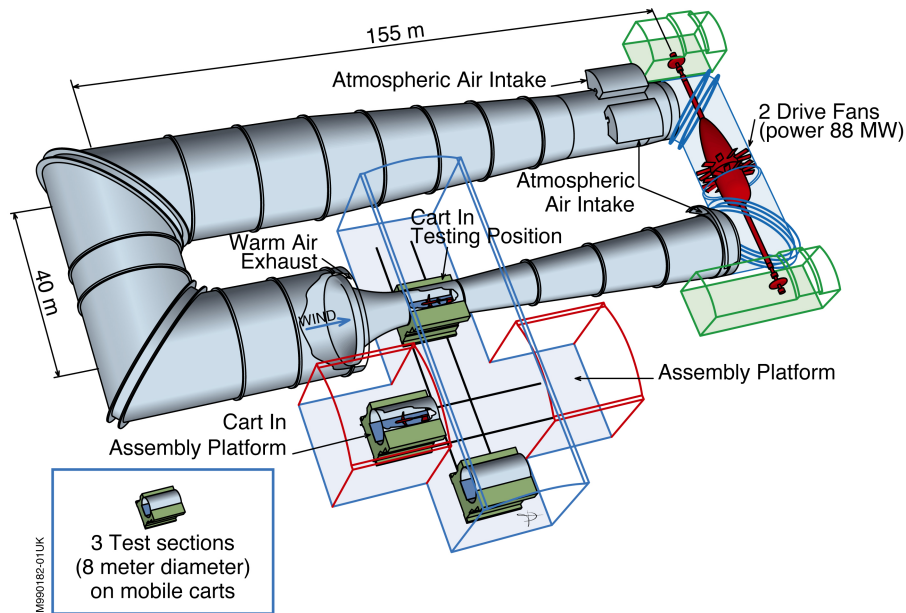


Fig. 1 S1MA wind tunnel aerodynamic circuit

of the facility's overall energy efficiency and for environment concerns allowing S1MA to be considered as a "green" test facility. The fans have fixed pitch and Mach numbers up to Mach 1 can be achieved, by varying the water mass flow and consequently the fan rotational speed (maximum RPM 230). For vibration considerations, the upstream fan is equipped with 12 blades while the downstream fan has 10 blades. Rotors and blades are made from steel and the edges are composites. To maintain the tunnel stagnation temperature below 60°C, two large atmospheric air intakes are located downstream of the fans. The air covers a distance of about 200 m from the fans before reaching a series of metal screens (honey-comb) that smooth and condition the air flow just before it enters the vast settling chamber (24 m - 79 feet in diameter). After passing the settling chamber, part of the air is exhausted via the air exhaust while the main part crosses successively the contraction, the test section, the diffuser and a corner equipped with vanes before coming back to the fans. The schematic of the tunnel circuit in Fig.1 shows the three interchangeable test sections. Then, one test is carried out while two others are prepared, which enables good tunnel productivity. Stagnation pressure is equal to the atmospheric pressure, i.e. usually around 0.9 bar; stagnation temperature stands between 263 and 333 K according to Mach number and atmospheric temperature. Reynolds number per meter for a 333 K stagnation temperature is $\approx 12 \cdot 10^6$.

This closed circuit, continuous flow wind tunnel can accommodate large-scale models, which permits the implementation of numerous experimental techniques. Typical tests, carried out in S1MA, are full and half model airframe tests and laminarity technology tests (natural laminar flow or hybrid laminar flow control). High pressure air distribution (200 bar, 17 kg/s) enables aeroacoustic propeller tests including CROR (Counter Rotating Open Rotor)

configurations or UHBR fan simulator. The laminarity tests and the acoustic measurements are highly impacted by the background noise of the facility.

In order to improve the acoustic quality of the wind tunnel, the applied strategy is to isolate the main acoustic source that contributes to the background noise in the test section. The main contributors to the background noise are the fan noise, the turning vane aerodynamic design and the turbulence screen. These types of studies have been previously conducted [6, 7]. It was decided that a complete redesign of the fan was outside the scope of the current study. Instead, the goal was to reduce the noise coming from the fans since this reduction should favorably impact the test section background noise. As the turning vane has to be upgraded for maintenance reasons, the idea is to redesign its structure to integrate an acoustic liner at the pressure side, therefore reducing the noise coming from the fans in the test section. In order to assess the concept, the cost and the efficiency of the turning vane liner, several simulations and a demonstrator have been set up. Figure 2 highlights the corner to be acoustically treated (corner #1) and the location of the demonstrator tested in this study

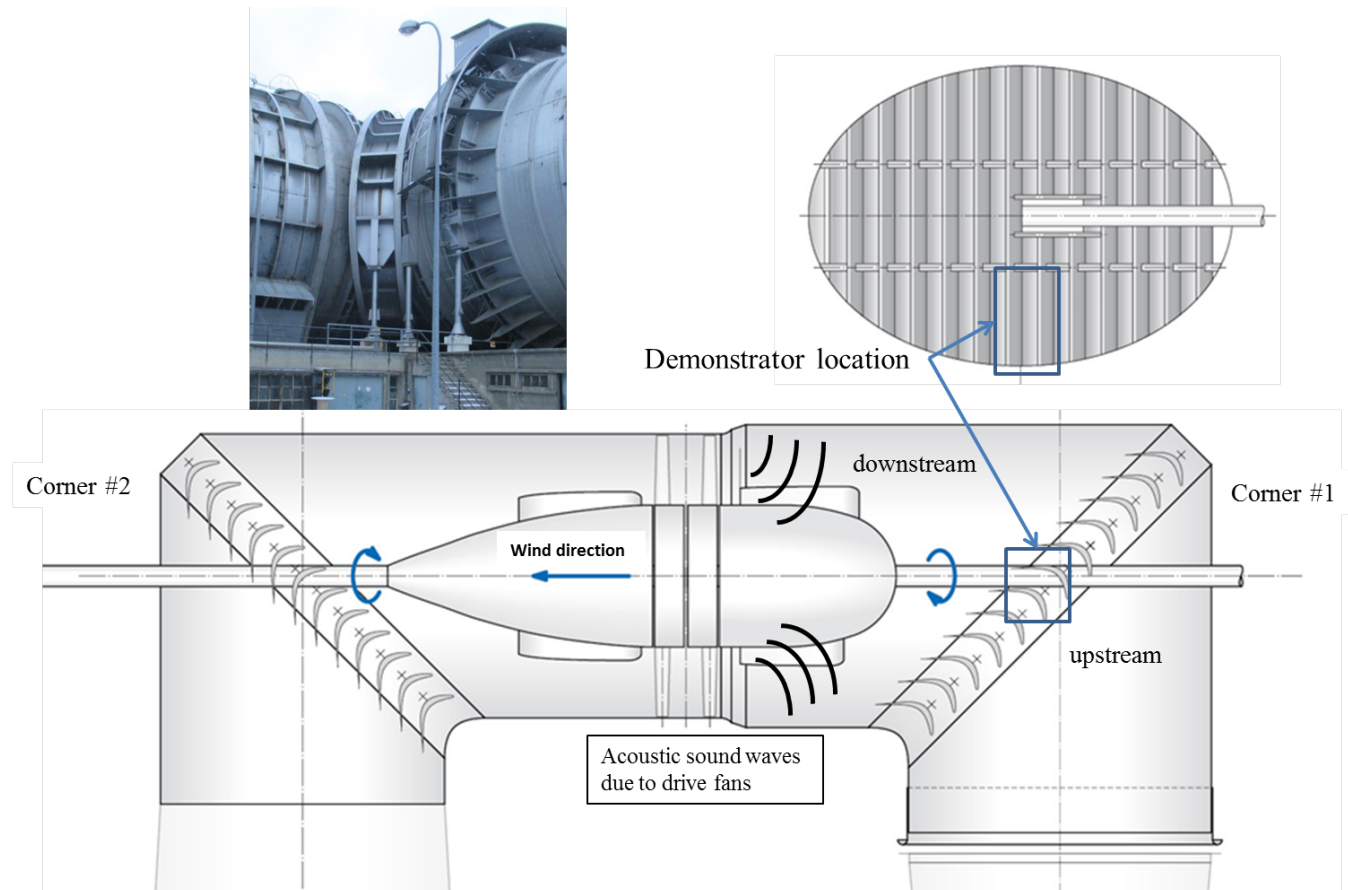


Fig. 2 Picture and schematic view of the first corner and the location of the demonstrator

III. Liner design procedure and simulation

A simplified 2D mesh was made in the horizontal plane of the wind tunnel turning vane, and is detailed in Fig. 3. The arrow indicating the direction of flow in Fig. 3 is placed for information to visualize where the upstream and downstream are located. In practice, no flow is considered in the simulations.

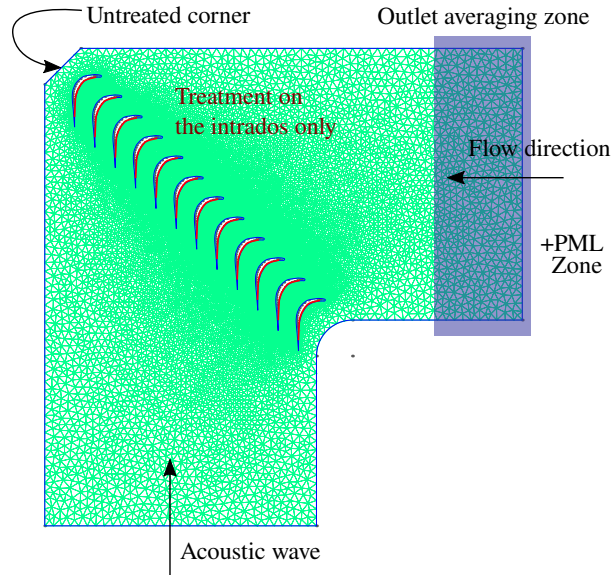


Fig. 3 Mesh of the studied configuration

The in-house code used, coined Space [12], is a Discontinuous-Galerkin (DG) calculation code allowing the solution of linearized Euler equations (LEE) in harmonic or temporal form. In the harmonic mode, a single excitation frequency is considered and a linear system is solved to find the sound field at each point. In time domain, a wider band signal can be considered. In the latter case, an impedance model is required to calculate the pressure-velocity convolution (with delay and fractional operators) at the impedance boundary condition. As these models are not yet integrated into Space, only harmonic calculations have been performed. For each frequency of interest, therefore, the optimal impedance for the reduction of the output sound pressure levels (SPL) is evaluated. At the inlet, a wave of mode order 1 is generated (a mode of order 0 corresponds to a plane wave). The reason for this choice of mode order relates to its spatial energy distribution. In the case of a ducted fan, most of the sound energy is concentrated towards the tip of the fan blades and there is almost no energy along the axis of the flow [13]. In the current work, a first (rough) approximation is made to represent this energy distribution by considering a higher-order mode. Here, the acoustic output (i.e., a non-reflecting boundary condition coupled with a PML zone) is on the right-hand side of Fig. 3, which would correspond to a flow-inlet condition if a flow were present. Views of the SPL fields for selected frequencies are given for information in Fig. 4,5 and 6. For each figure, two configurations are presented with the left plot showing results when the upper left corner is untreated and the right showing the effect of treatment in that corner. A salient point of these latter simulations is the “leakage” observed when the corner is left untreated.

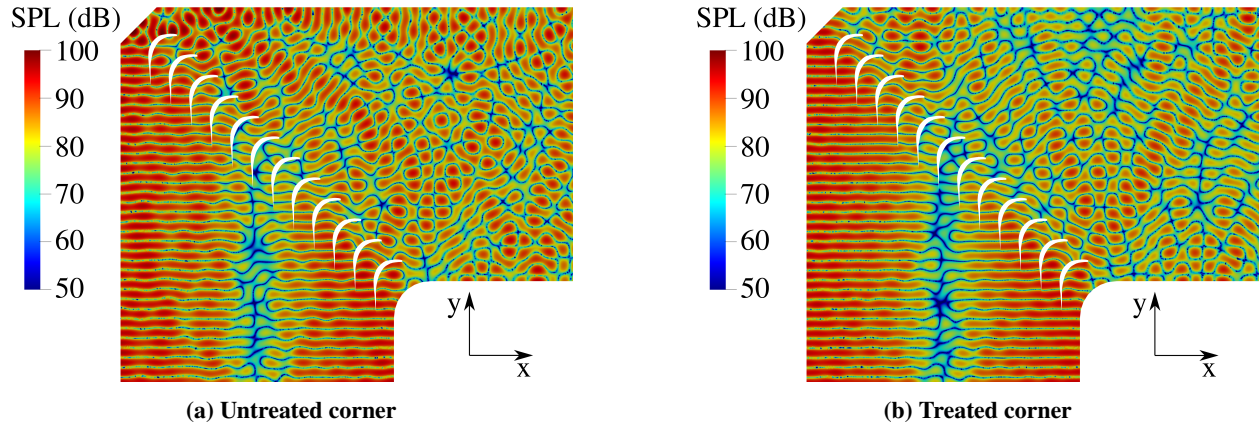


Fig. 4 Sound pressure field simulations results in the turning vane at 300 Hz

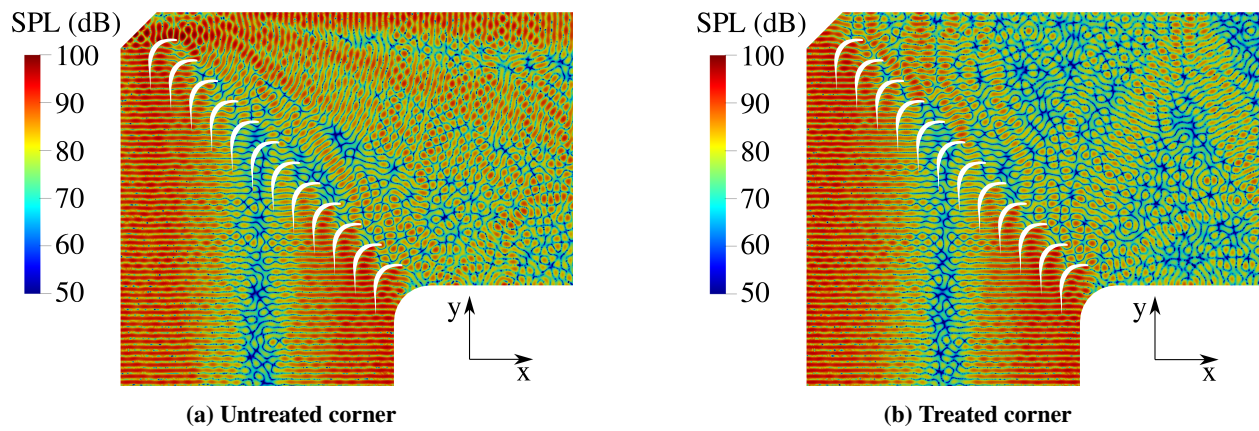


Fig. 5 Sound pressure field simulations results in the turning vane at 500 Hz

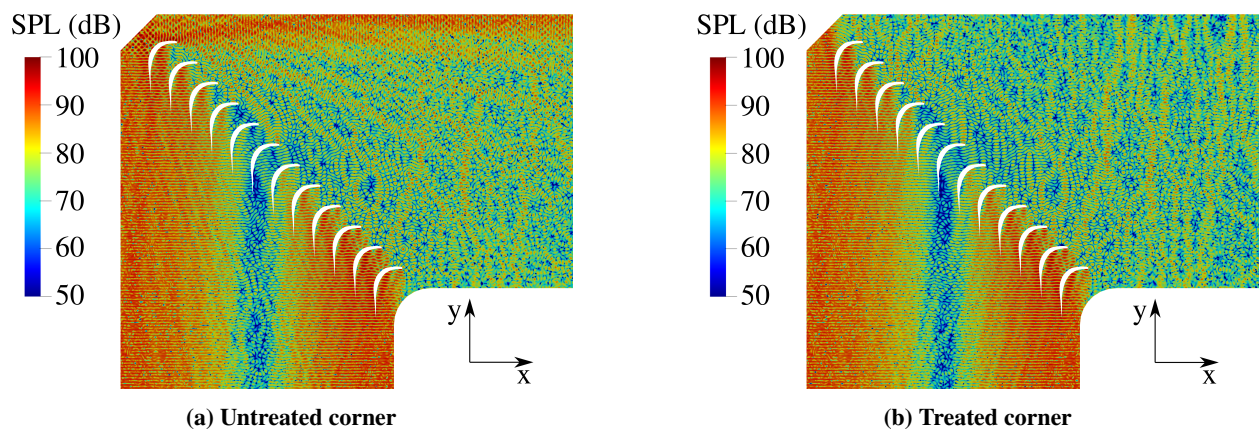


Fig. 6 Sound pressure field simulations results in the turning vane at 1000 Hz

A. Generating impedance maps

For each frequency of interest, simulations were performed with several impedance values. In each case, the output average SPL was recorded (the average is conducted on the acoustic pressure, before converting to a SPL). The first step is to compute the output level as a function of liner impedance. This provides an optimum impedance (the one that gives the smallest output level) for each frequency of interest. The second step is to use an optimizer with a liner model to determine which configuration provides the closest impedance to the optimum (as a function of frequency). It is similar to Nark et al. approach [14]. It is indeed faster to use an optimization loop on material models giving an impedance as an output, and interpolate this impedance on the pre-calculated maps, rather than redoing a full calculation each time. This saves several orders of magnitude in terms of calculation time, as the impedance calculation is of the order of a millisecond, compared with several tens of minutes for Space to calculate the attenuation at a given impedance (sometimes several hours, depending on the mesh, which needs to be finer when high frequencies are considered, due to a reduced wave length).

For each frequency, Figs. 7, 8 and 9 show the associated impedance maps, as well as the output SPL averaged along the x axis over 3 m in the axial direction (see blue area in Fig. 3).

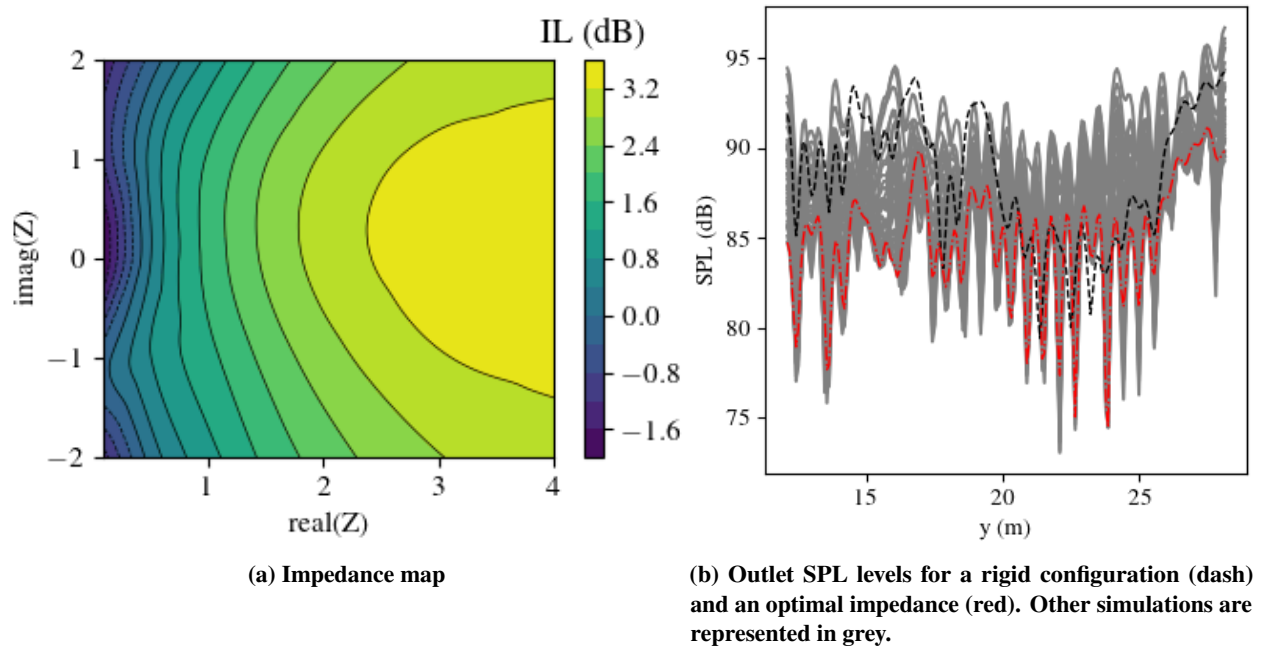


Fig. 7 Impedance map and associated SPLs at 300 Hz

The SPL is plotted for a "rigid" configuration where the impedance is $+\infty$ (rigid wall case, black line in the figures), and for all impedances used in the calculation of the map (grey lines). In red, the output level associated with the optimal impedance for this frequency is plotted. Note that, since the optimal impedance value refers to a pressure averaged over the entire zone depicted in Fig. 3, it is thus not necessarily optimal at each value of y . This explains why

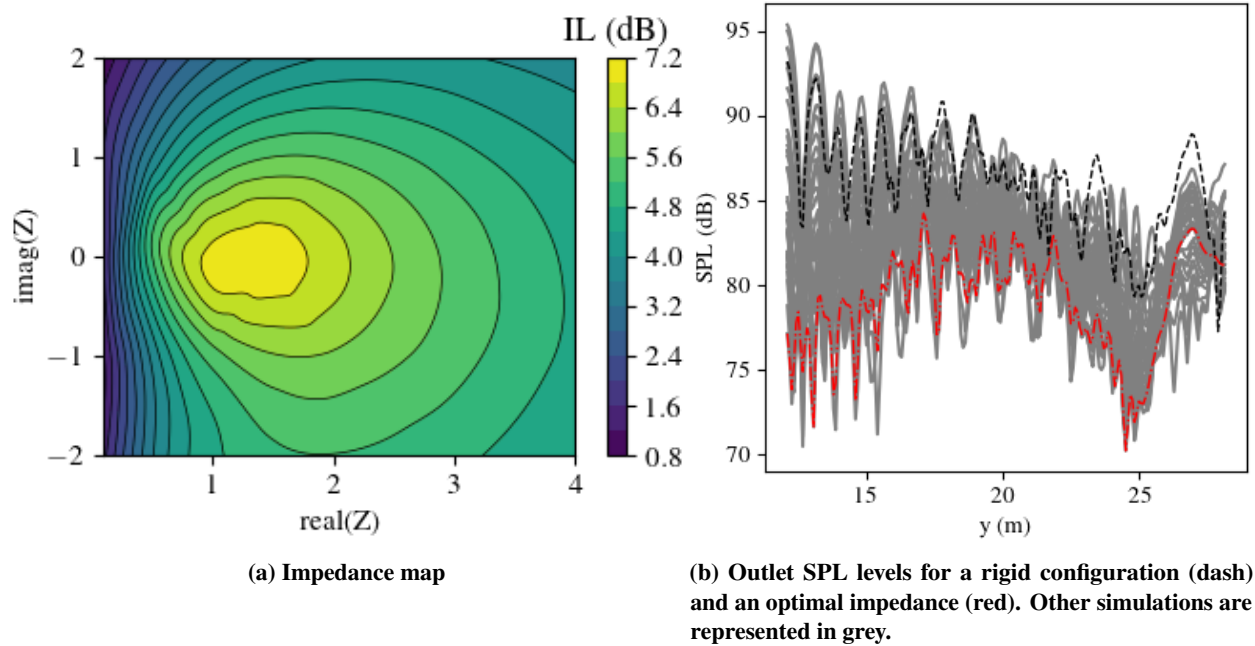


Fig. 8 Impedance map and associated SPLs at 500 Hz

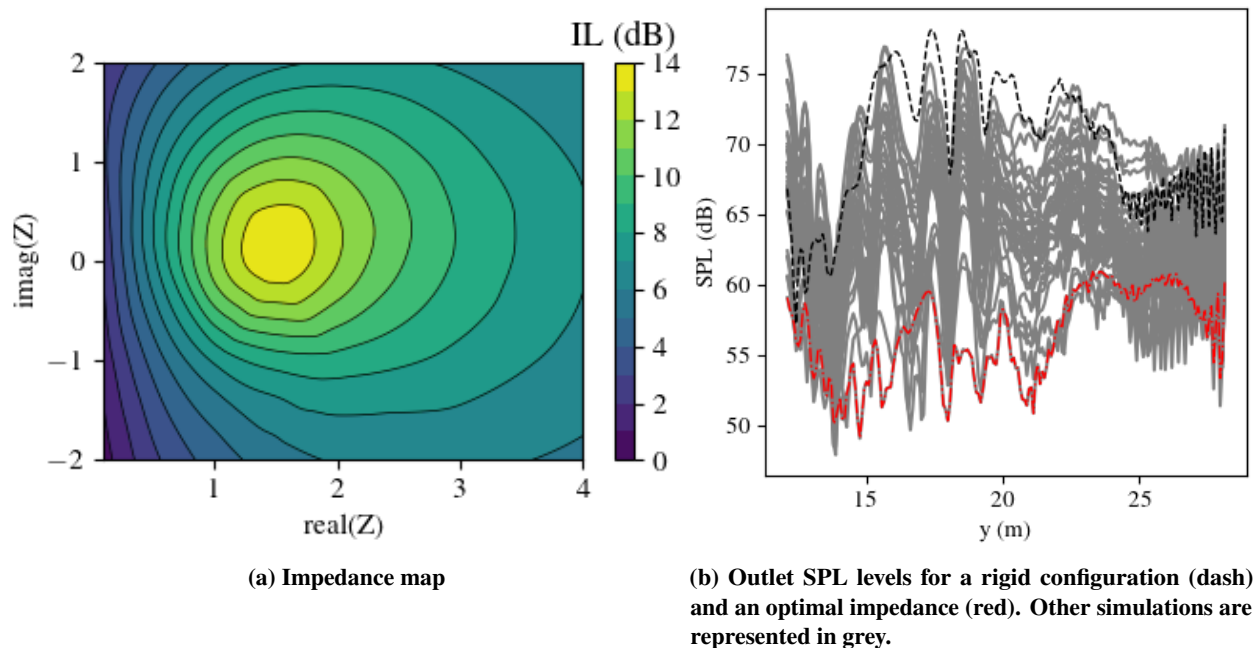


Fig. 9 Impedance map and associated SPLs at 1000 Hz

for a given value of y , certain impedances (grey lines) can locally display a lower SPL than the optimal (red line). The impedance maps represent the insertion loss (IL) in dB: a first call to the high fidelity solver is done with a fully rigid liner (i.e., $Z = +\infty$), and the average SPL at the output is recorded. The difference between this average SPL and the subsequent ones, obtained with different values of Z , is the IL represented on the maps. Positive values mean that a

reduction in the output SPL was attained on average.

B. Selected liner design

The optimal impedance as a function of frequency is plotted in Fig. 10. Apart from very low frequencies, the impedance values are relatively constant. This poses a problem for the design from the outset, as most known solutions (single degree of freedom liners) do not offer this kind of impedance. The issue at very low frequency is probably caused by two factors: (i) the impedance map is very flat, meaning that a large range of impedances give virtually the same output, and (ii) the averaging zone might not extend enough for the average in pressure to be meaningful at these frequencies. The latter issue could be resolved by extending the mesh in the x direction.

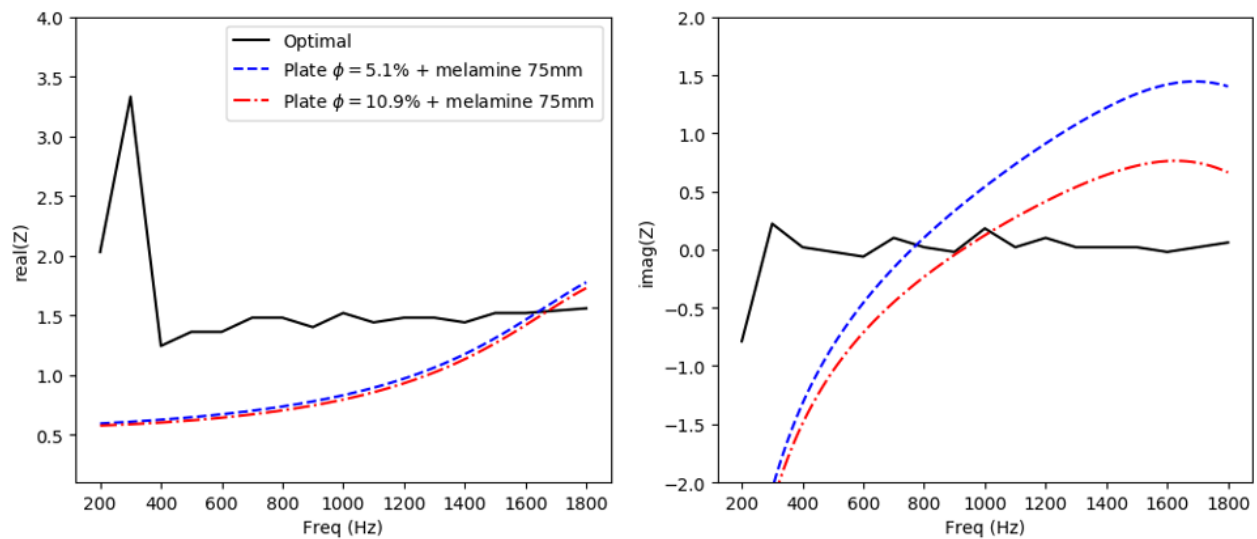


Fig. 10 Optimal impedance as a function of frequency. Real (left) and imaginary (right) part. Also shown are the impedances of the two liners made, considering a given thickness of acoustic foam

In view of the integration mechanical constraints on the vanes, it was decided to keep the design of the liner simple, by creating a single degree of freedom liner composed of a porous acoustic foam and a perforated sheet with internal partitions to inhibit extended reactions. This type of design allows for medium and high frequency absorption. To improve the concept in terms of robustness with minimal modifications, it was proposed to alternate perforated sheets with different porosities along the profile chord. This configuration draws inspiration from the concept of metasurfaces where different liners can be placed in parallel to extend the range of absorption of the sample.

As there are still many unknowns (modal content of the source, velocity profile of the flow on the blades), it seemed appropriate to diversify the solution as much as possible. Two different facesheet porosities were tested. These plates have a thickness of 1 mm and a perforation diameter of 1.5 mm. During the prototype tests, six configurations were mounted:

- rigid plate,

- perforated plate with porosity 1, with rigid partitions in the foam
- perforated plate with porosity 2, with rigid partitions in the foam
- alternating perforated plates porosities: 1-2-1-2 from downstream to upstream (0.75m chordwise), relative to the flow, with rigid partitions in the foam
- perforated plate with porosity 1, with cut foam without any partition
- perforated plate with porosity 1, with a full piece of foam

The last two configurations have been tested because they are of interest for an easy technical implementation. The liner design for the turning vane blades is a highly constrained case, which makes an attempt at optimization difficult. Work with Space on partial modeling of this part of the wind tunnel has, however, shown the potential benefit of treating the outer corner.

Different variable elements of the simulation can be taken into account: the thickness of the foam, which varies along the vane (value between 40 and 100 mm); the local Mach speed, which varies between about 0 and 0.15 and the overall sound pressure level (SPL). If we use all these values as bounds in the liner model (accounting for nonlinear behavior in SPL and Mach), we can plot the impedance as a function of frequency with associated standard deviations, see Fig. 11. Note that the flow was neglected in the Space simulations leading to the impedance map, but that it was still considered in the models linking the geometrical properties of the liners to their impedance.

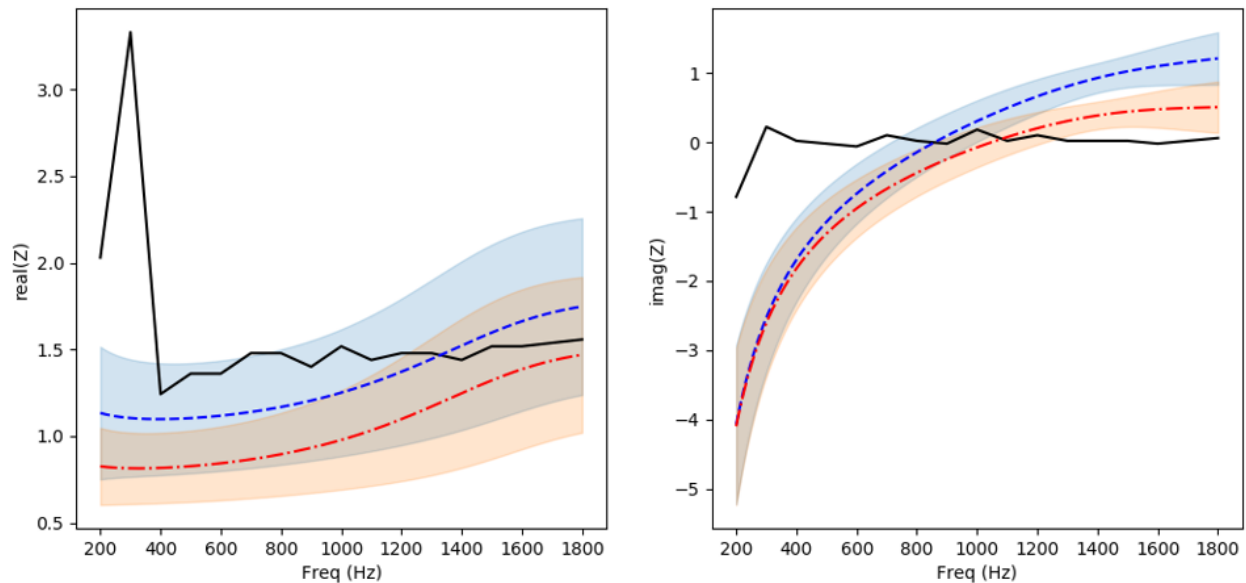


Fig. 11 Real and imaginary parts of the impedance. In black, the optimal target impedance. In blue, the impedance theoretically realized by liner 1. In red, the impedance theoretically realized by liner 2. The dotted lines correspond to an average, carried out over 1000 samples.

Local nonlinear effects at the perforations of the liner, induced by high sound levels or grazing flow, tend to increase the resistance value. The liner was thus chosen to have the optimal impedance characteristics at the target Mach number

and SPL. A prior test campaign allowed us to identify these targets.

IV. Experimental set up and post-processing

1. Lined turning vane demonstrator and instrumentation



(a) Leading edge

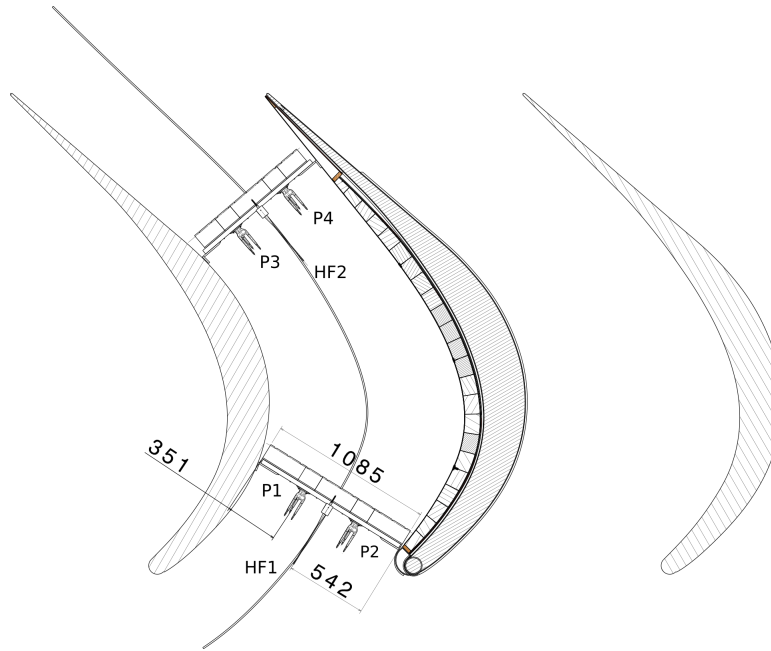


(b) Trailing edge

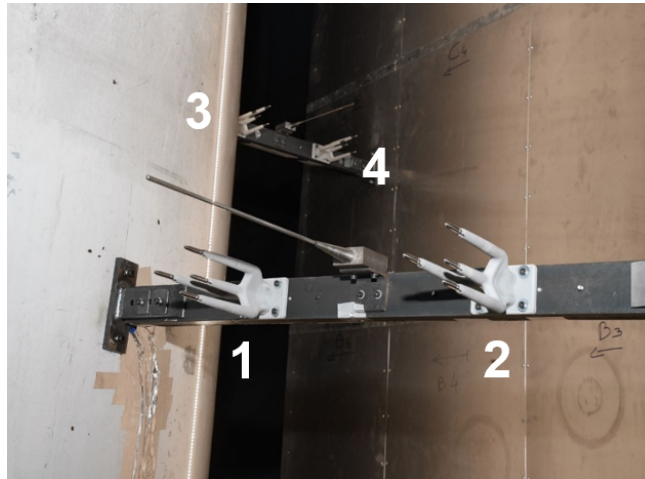
Fig. 12 View of the liner demonstrator installed in the the turning vane

Figure 12 presents the demonstrator placed on a part of the turning vane. The demonstrator is placed on the pressure side of a turning vane and covers the full chord of the turning vane and 4 m spanwise. The demonstrator is superimposed to the existing turning vane. This demonstrator is composed of an acoustic foam which covers the turning vane fixed on a wood structure. Over the foam, a reference configuration with a flat plate is available in order to have a reference value. Several perforated plates with different porosities can also be considered. One can alternate the different perforated plates and study the effect of each configuration.

In order to assess the effect of the acoustic liner, a specific, in-flow 3D intensity probe called "cactus probe" has been developed. Each probe is composed of four microphones mounted with a nose cone. This mounting enables to compute the intensity measured for a given position. The intensity value is more robust than local SPL measurements in order to correctly evaluate the noise reduction effects of the liner. These probes overall dimensions are 175 mm long and 61 mm large. Hot film probes are used to measure the local velocity. Figure 13 is a picture of the setup. Probes 1 and 2 are upstream, near the leading edge of the turning vane. Probes 3 and 4 are downstream at the leading edge of the turning vane. These two probes are firstly impacted by the noise due to the windtunnel drive fans. The intensity probes support beams are placed at a different height in order to avoid any interaction with potential downstream wakes. Therefore, trailing edges have been added behind the support beam in order to minimize spurious noise due to the wake. One can see, in between the two upstream intensity probes, the hot film probe to accurately measure the flow velocity which is rather low at these positions in the windtunnel. Figure 13a shows the assembly used with some characteristic dimensions



(a) Sketch of the experimental set-up : the cactus probes are denoted P_i and the hotfilm probes are denoted HFi , the dimensions are given in millimeter.



(b) In-flow intensity probes picture

Fig. 13 Experimental set-up and instrumentation

that allow to evaluate the possible interactions between the measuring devices and shows the liner demonstrator in its partitioned configuration. The foam thickness is around 100mm and the partition is a square of 130mm side.

2. In-flow intensity probe post-processing

Based on Morfey's intensity formulation [15], Munro and Ingard [16] proposed an intensity I formulation in presence of a mean flow based on the autospectra (G_{11} and G_{22}) and crossspectra (G_{12} of 2 microphones (# 1 and # 2)

separated by a distance Δl . This formula writes

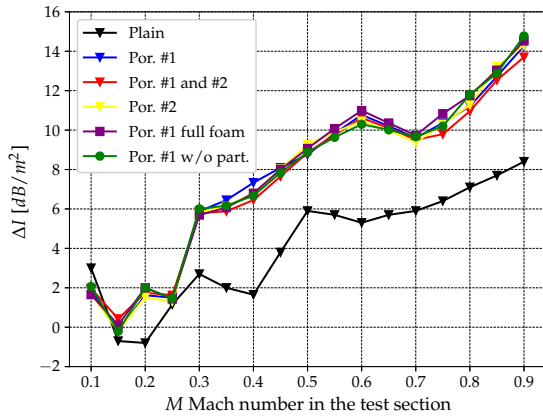
$$I(\omega) = -\frac{(1 - M_0^2)(1 + 3M_0^2)}{\omega\rho_0\Delta l} \Im(G_{12}) + \frac{M_0(1 + M_0^2)}{2\rho_0 c} (G_{11} + G_{22} + 2\Re(G_{12})) + \frac{M_0(1 - M_0^2)^2 c}{\rho_0(\omega\Delta l)^2} \frac{(G_{22} - G_{11})^2 + 4(\Im(G_{12}))^2}{G_{11} + G_{22} + 2\Re(G_{12})}, \quad (1)$$

with M_0 the uniform local Mach number, ρ_0 the fluid density, c the sound celerity and ω the frequency pulsation. Camparin [17] experimentally assessed this approach while [18] proves by experimentation that the intensity with flow formulation as, cost function, is more relevant than pressure fluctuations to reduce the propagated noise with active control process. The 3D intensity norm can be assessed by applying, for each probe direction, Equation (1): it is applied successively between each of the three outer mics (#2) and the center mic (#1). The results are projected in an orthonormed axis system with the proper projection of the Mach number in each direction. The cactus probes are assumed to be placed in a mean flow which remains constant. The local Mach Number is assessed using a local velocity measurement.

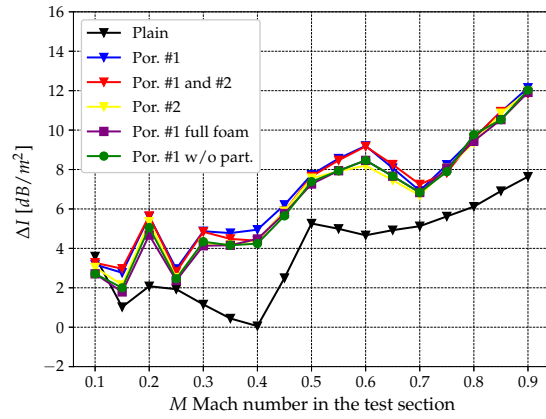
V. Acoustic efficiency of the demonstrators

A reference test campaign has been performed prior to the demonstrator test campaign in order to have a reference configuration without anything on the turning vane. The probes are placed at the exact same locations for the different configurations (with and without the demonstrator). Figure 14 and Figure 15 present the difference between the reference configuration intensity and the lined turning vane configurations intensity integrated from 500 Hz up to 2000 Hz upstream and downstream, respectively. The lower bound is thus chosen because it corresponds to the specifications requested by the wind tunnel division. The upper bound is selected with regard to the theoretical limitation imposed by the geometrical definition of the acoustic intensity probes. Only the modulus value of the intensity is considered. The Mach number for the abscissa corresponds to the Mach number in the test section. The Mach number in the test section is linearly linked to the drive fans RPM, thus the noise source increases with the Mach number. Indeed, for a given Mach number in the test section, the local Mach number in the wind tunnel corner ranges from 0 up to 0.15. As the main goal is to reduce the background noise in the test section, it is interesting to assess the efficiency of the liner for the Mach number in the test section.

The six configurations have been tested in order to correctly assess the effect of the liner demonstrator and thus its efficiency. It is important to underline the limitation of the experimental setup : the instrumentation allows only two locations for each position (upstream and downstream). It is insufficient to assess a real insertion loss since the upstream and downstream probes are not on the same intensity stream-trace. Moreover, the liner demonstrator increases

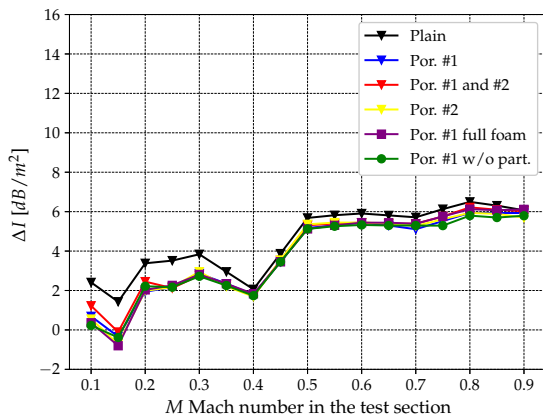


(a) Upstream probe 1

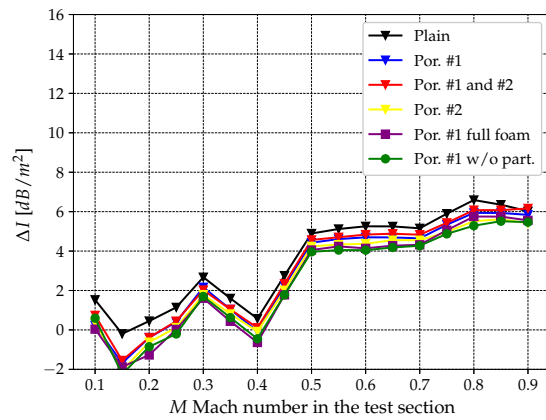


(b) Upstream probe 2

Fig. 14 Upstream overall intensity level ΔI from 500 Hz up to 2000 Hz difference between reference configuration and the demonstrator configuration



(a) Downstream probe 3



(b) Downstream probe 4

Fig. 15 Downstream overall intensity level ΔI from 500 Hz up to 2000 Hz difference between reference configuration and the demonstrator configuration

the thickness of the pressure side of the turning vane: the flow and, thus, the acoustic field are modified. The excess thickness set up explains the apparent noise reduction observed between the reference configuration and the plain configuration: the sound field is modified. One can also notice that the upstream overall intensity level difference is significantly higher than the downstream corresponding set of data, while the downstream results remain insensitive to the liner configuration. It confirms that the incoming noise source finds its origin in the wind-tunnel fans. Considering that the only noise contribution to the wind-tunnel test section can be assessed by the upstream set of data, it can be used to show the efficiency of the different demonstrators. The efficiency of the liner increases with Mach number which was anticipated from the liner optimisation. The results are satisfactory and validated the design. The lack of number of

additional spatial measurements thwart assessing the effect of different tested configurations and the partitioning inside the liner. Regarding the upstream probes in Figure 14, the difference between the reference configuration and the lined configurations highlighted an insertion loss of several dB. The liner seems to produce a sufficient noise reduction in order to consider the next step: the redesign of the turning vane with the liner at the pressure side of the turning vane.

VI. Conclusions

This engineering note proposes the complete procedure including the optimization, design and evaluation of an acoustic liner demonstrator for the treatment of the turning vane in the S1MA wind tunnel. This modification is proposed to reduce the background noise in the test section. Local measurements of the acoustic attenuation obtained from a liner demonstrator enable risk reduction for future investments. The different tested configurations are satisfactory in terms of expected attenuation. This study provides the end-to-end implementation of the different simulation and measurement tools allowing the evaluation of acoustic liners under very demanding industrial conditions. After the complete corner modification, measurements in the test section will be made to quantify the final background noise reduction.

Acknowledgments

The authors wish to thank Timothée Chabert and the S1MA team for running the tests. This study was performed in the framework of RAMSES, project funded by the Direction Générale de l'Aviation Civile. The second author wishes to thank Christophe Peyret for his help in setting up the DG simulations.

References

- [1] Chung, J. Y., "Rejection of flow noise using a coherence function method," *The Journal of the Acoustical Society of America*, Vol. 62, No. 2, 1977, pp. 388–395. <https://doi.org/10.1121/1.381537>, URL <https://doi.org/10.1121/1.381537>.
- [2] Blacodon, D., "Spectral estimation method for noisy data using a noise reference," *Applied Acoustics*, Vol. 72, No. 1, 2011, pp. 11–21. <https://doi.org/https://doi.org/10.1016/j.apacoust.2010.09.004>, URL <https://www.sciencedirect.com/science/article/pii/S0003682X10002082>.
- [3] Blacodon, D., and Mohammad-Djafari, A., "Separation of acoustical source power spectral densities with Bayesian sparsity enforcing," *Journal of Sound and Vibration*, Vol. 480, 2020, p. 115334. <https://doi.org/https://doi.org/10.1016/j.jsv.2020.115334>, URL <https://www.sciencedirect.com/science/article/pii/S0022460X20301656>.
- [4] Fleury, V., Coste, L., Davy, R., Mignosi, A., Cariou, C., and Prosper, J.-M., "Optimization of Microphone Array Wall Mountings in Closed-Section Wind Tunnels," *AIAA Journal*, Vol. 50, No. 11, 2012, pp. 2325–2335. <https://doi.org/10.2514/1.J051336>, URL <https://doi.org/10.2514/1.J051336>.
- [5] Remillieux, M., Crede, E., Camargo, H., Burdisso, R., Devenport, W., Rasnick, M., Seeters, P. V., and Chou, A., "Calibration

- and Demonstration of the New Virginia Tech Anechoic Wind Tunnel,” *14th AIAA/CEAS Aeroacoustics Conference (29th AIAA Aeroacoustics Conference)*, 2008. <https://doi.org/10.2514/6.2008-2911>, URL <https://arc.aiaa.org/doi/abs/10.2514/6.2008-2911>.
- [6] Bergmann, A., “The Aeroacoustic Wind Tunnel DNW-NWB,” *18th AIAA/CEAS Aeroacoustics Conference (33rd AIAA Aeroacoustics Conference)*, 2012. <https://doi.org/10.2514/6.2012-2173>, URL <https://arc.aiaa.org/doi/abs/10.2514/6.2012-2173>.
- [7] Holthusen, H., Bergmann, A., and Sijtsma, P., “Investigations and measures to improve the acoustic characteristics of the German-Dutch Wind Tunnel DNW-LLF,” *18th AIAA/CEAS Aeroacoustics Conference (33rd AIAA Aeroacoustics Conference)*, 2012. <https://doi.org/10.2514/6.2012-2176>, URL <https://arc.aiaa.org/doi/abs/10.2514/6.2012-2176>.
- [8] Mery, F., Rey, M., Davy, R., and Fernando, R., “Far field wall-mounted microphone device for the S1MA anechoic closed-section wind tunnel applied to Open Rotor,” *18th AIAA/CEAS Aeroacoustics Conference (33rd AIAA Aeroacoustics Conference)*, 2012. <https://doi.org/10.2514/6.2012-2228>, URL <https://arc.aiaa.org/doi/abs/10.2514/6.2012-2228>.
- [9] Mery, F., Davy, R., Fleury, V., Bulte, J., and Rey, M., “Beamforming-based noise level dereverberation solution for S1MA sonic wind-tunnel : metrology, methodology and validation,” , 2015. <https://doi.org/10.2514/6.2015-3274>, URL <https://arc.aiaa.org/doi/abs/10.2514/6.2015-3274>.
- [10] Nicolas, F., and Rey, M., “S1MA Wind Tunnel New Aeroacoustic Capability: a Traversing Microphone Array,” *2018 AIAA/CEAS Aeroacoustics Conference*, 2018. <https://doi.org/10.2514/6.2018-3137>, URL <https://arc.aiaa.org/doi/abs/10.2514/6.2018-3137>.
- [11] Mery, F., “A cross-comparison of different post-processing and acoustic measurement devices for high speed near field noise on the S1MA BHCR open rotor test rig,” *20th AIAA/CEAS Aeroacoustics Conference*, 2014. <https://doi.org/10.2514/6.2014-3317>, URL <https://arc.aiaa.org/doi/abs/10.2514/6.2014-3317>.
- [12] Léger, R., Peyret, C., and Piperno, S., “Coupled discontinuous Galerkin/finite difference solver on hybrid meshes for computational aeroacoustics,” *AIAA journal*, Vol. 50, No. 2, 2012, pp. 338–349. <https://doi.org/10.2514/1.J051110>.
- [13] B.D. Mugridge, C. M., “Sources of Noise in Axial Flow Fans,” *The Journal of the Acoustical Society of America*, Vol. 51, No. 1411, 1972. <https://doi.org/https://doi.org/10.1121/1.1912992>.
- [14] Nark, D. M., and Jones, M. G., “An acoustic liner design methodology based on a statistical source model,” *International Journal of Aeroacoustics*, Vol. 20, No. 5-7, 2021, pp. 441–457. <https://doi.org/10.1177/1475472X211023874>, URL <https://doi.org/10.1177/1475472X211023874>.
- [15] Morfey, C., “Acoustic energy in non-uniform flows,” *Journal of Sound and Vibration*, Vol. 14, No. 2, 1971, pp. 159–170. [https://doi.org/https://doi.org/10.1016/0022-460X\(71\)90381-6](https://doi.org/https://doi.org/10.1016/0022-460X(71)90381-6), URL <https://www.sciencedirect.com/science/article/pii/0022460X71903816>.
- [16] Munro, D. H., and Ingard, K. U., “On acoustic intensity measurements in the presence of mean flow,” *The Journal of the Acoustical Society of America*, Vol. 65, No. 6, 1979, pp. 1402–1406. <https://doi.org/10.1121/1.382926>, URL <https://doi.org/10.1121/1.382926>.

[17] Comparin, R. J., Rapp, J. R., and Singh, R., "Measurement of acoustic intensity in the presence of one-dimensional fluid flow," *The Journal of the Acoustical Society of America*, Vol. 72, No. 1, 1982, pp. 7–12. <https://doi.org/10.1121/1.388027>, URL <https://doi.org/10.1121/1.388027>.

[18] Simon, F., "Adaptive active control of acoustic intensity in flow," *Internoise 2012*, 2012.